Supplementary information

Mechanically stable ternary heterogeneous electrodes for energy storage and conversion

Libo Gao[1,2], Hongti Zhang[1,2], James Utama Surjadi[1], Peifeng Li[3], Ying Han[1], Dong Sun[1], Yang Lu[1,2]*

[1] Department of Mechanical and Biomedical Engineering, City University of Hong Kong, Hong Kong SAR, Kowloon 999077, Hong Kong;

[2] Shenzhen Research Institute, City University of Hong Kong, Shenzhen 518057, China

[3] College of Materials Science and Engineering, Shenzhen University, Shenzhen 518060, China

*Author to whom correspondence should be addressed;

E-Mail: yanglu@cityu.edu.hk

Experimental

Preparation of FeCo@NiCo-LDH

The FeCo-LDH@NiCo-LDH was fabricated via a facile successive electrodeposition method with potentiostatic mode under -1 V vs SCE. Typically, after treated with the acetone, ethanol and 3 M HCl solution for 15 min, respectively, the pre-treated nickel foam (NF) was initially coated with a thin FeCo-LDH film for 15 min in an electrolyte consisting of 4 mM $Co(NO_3)_2 \cdot 6H_2O$ and 4 mM $FeSO_4 \cdot 7H_2O$. Following by drying the sample in air at 65 °C, the NF coated with FeCo-LDH was directly used as the scaffold to deposit NiCo-LDH film for another 15 min. The electrolyte used for further deposition was analogous to the previous electrodeposition, consisting of 4 mM $Co(NO_3)_2 \cdot 6H_2O$ and 2 mM $Ni(NO_3)_2 \cdot 6H_2O$. Finally, the hierarchical heterogeneous FeCo@NiCo-LDH was dried at 65 °C for electrochemical test.

Preparation of negative electrode

In a typical procedure, the activated carbon (AC, 80 wt%, Japan) was mixed with carbon black (10 wt%) and polyvinylidene-fluoride (PVDF,10 wt%). After fully blended with a small amount of N-methylpyrrolidone (NMP) at 70 °C, the resulting mixture was coated on NF and pressured with drying in an oven at 70 °C for 12 h.

Structural Characterization

The morphology and structure were characterized by field emission scanning electron microscope (FESEM, Quanta 450) and transmission electron microscope (TEM, JEOL JEM 2100F) with energy dispersive spectroscopy (EDS). The X-ray powder diffractometer (XRD, RigakuSmartLab) with monochromatic Cu Kα (1.5418 Å) was employed to identify its phase structure.

in situ SEM Mechanical Characterization

Monotonic compression tests were performed on the samples inside SEM through a quantitative picoindentor (Hysitron^{TM} PI85). The samples were compressed using a diamond flat punch tip with 5 μm in diameter, with the load applied from the apex of the vertical axis, moving down at a constant prescribed displacement rate of 10 nm s^{-1}. Load-displacement

curves were recorded accordingly. By using the nominal cross-sectional area and height of the structure, engineering stress and strain would be obtained.

Electrochemical test

The electrochemical performance of the synthesized supercapacitor was analyzed in terms of the cyclic voltammetry (CV) and galvanostatic charge/discharge (GCD) as well as the electrochemical impedance spectroscopy (EIS) measurements of the positive and negative materials. Tests were conducted in a three-electrode system by using a platinum foil as the counter electrode, a saturated calomel electrode (SCE) as the reference electrode, and 2 M KOH as electrolyte.

For the positive electrode, the specific capacitance can be calculated based on the following equation:[1]

$$C = \frac{2i\int Vdt}{V^2\Big|_{Vi}^{Vf}} \quad (1)$$

On the other hand, the specific capacitance of the negative electrode can be calculated according to the following relation:

$$C = \frac{i\Delta t}{m\Delta V} \quad (2)$$

Where i (A) is the areal or mass current density, Vi (V) and Vf (V) is the initial and final voltage during discharging process, t or Δt (s) is the discharge time and V (V) is the potential range.

For the assembled two-electrode system, the charge balance was obtained according to following equation:[2]

$$\frac{m_+}{m_-} = \frac{\left(\int idV/v\right)_-}{\left(\int idV/v\right)_+} \quad (3)$$

Where m_+ (m_-) is the mass loading, v (mV s^{-1}) is the scan rate, V (V) is the voltage and $\int idV$ is the integral area of the cyclic voltammogram for the positive or negative electrode at 5 mV

s^{-1}. According to the equation, the mass ratio of the positive electrode to positive electrode was found to be 1:3.18. The total mass of the ASC was determined to be 6.27 mg cm^{-2}, based on the specific masses of the positive and negative electrodes, which were 1.5 mg cm^{-2} and 4.77 mg cm^{-2} respectively. The detailed assembly procedure of the solid ASC is similar with our previous work.[3] Typically, 3 g of PVA was dissolved in 20 mL of distilled water with stirring at 90 °C, when it became transparent followed by adding 10 mL of 0.3 g mL^{-1} KOH slowly. With further stirring for 4 h, the positive and negative electrodes were both immersed into the gel electrolyte for 5 min, respectively. Finally, they were assembled together after becoming solid in air temperature with following immersed into the gel electrolyte again and protected with a Kapton film.

The specific capacitance was obtained by using equation (1). The energy density (E, Wh kg^{-1}) and power density (P, W kg^{-1}) can be calculated by the following relations,

$$E = \frac{1}{2} \times CV^2 \tag{4}$$

$$P = \frac{E}{t} \tag{5}$$

Where C (F g^{-1}) is the specific capacitance, V (V) is voltage range of the ASC, and t (s) is corresponding discharge time.

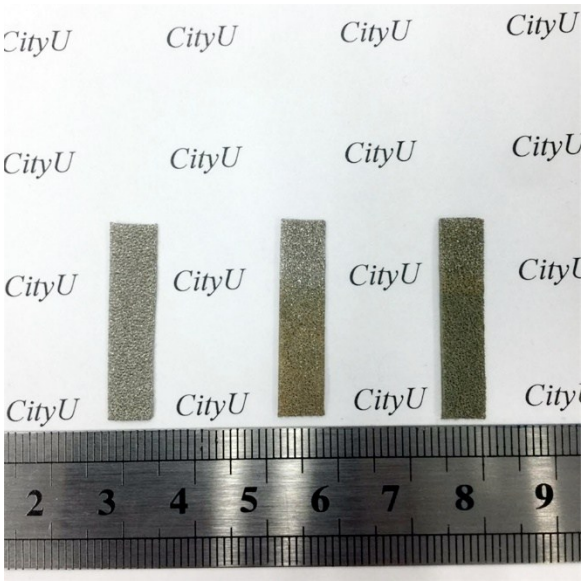

Figure S1. Digital optical images of the pure nickel foam, FeCo-LDH and FeCo@NiCo-LDH.

As shown in Figure S2, the FeCo-LDH and FeCo@NiCo-DLH both exhibit typical (003), (006), (012) and (110) peaks of LDH phase (JCPDS 51-0045) after electrodeposition.[4] But the signals of the FeCo@NiCo-LDH is stronger than that of the FeCo-LDH, indicating the successful synthesis of the hierarchical structure.

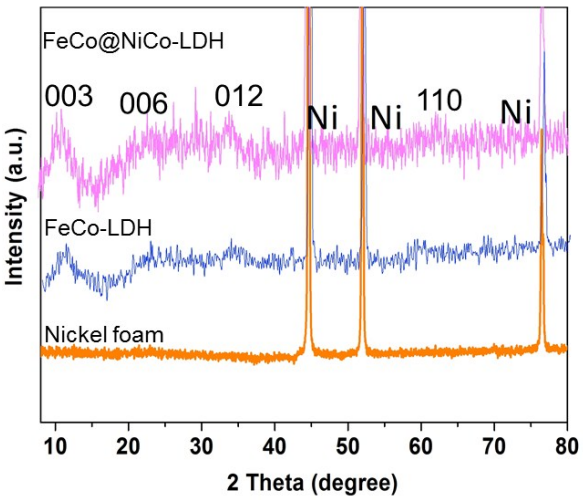

Figure S2. XRD patterns of the nickel foam, FeCo-LDH and FeCo@NiCo-LDH, respectively.

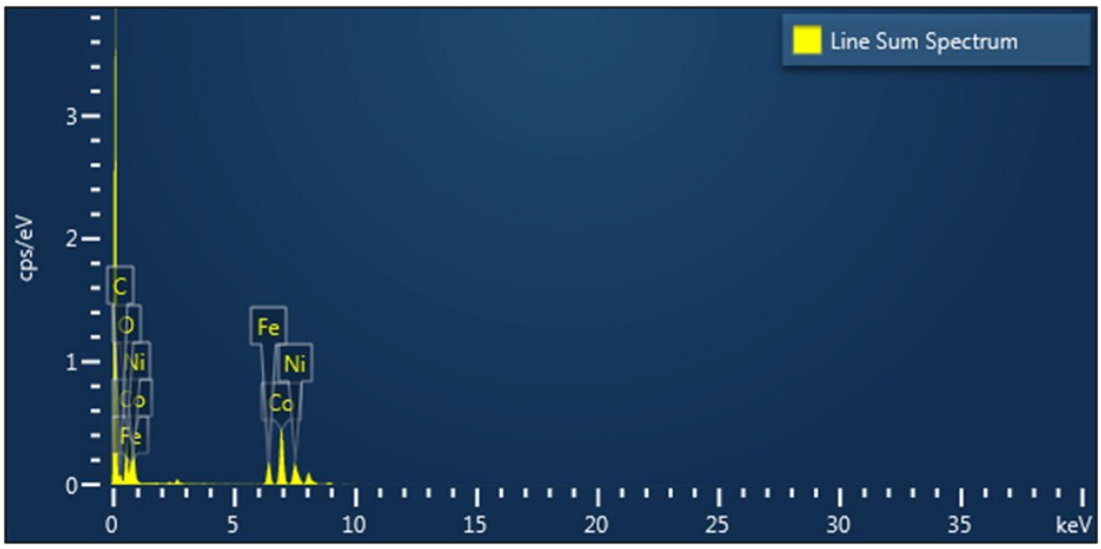

Figure S3. TEM-EDS of the FeCo@NiCo-LDH.

The loading-unloading micro-test was employed with a picoindentor at a speed rate of 10 nm s^{-1} with a diamond flat punch tip with 5 μm in diameter. In these tests, two different kind of modes was used. As shown in Figure S4a, four cycles of loading-unloading tests with the same compressive strain almost have the same slope, this indicates that the composite exhibit the same Young's modulus, demonstrating that the sample has minor cracking occurred. Importantly, no any force drops happened during the test process, which means the NiCo-LDH has a very good bonding on the FeCo-LDH. And this is also further confirmed by the cyclic test with different compressive strain (20%, 30%, 40%, 50%). As shown in Figure S4b, after each loading test, the curves still can almost remain the same trend with following the prior test, which demonstrate the good recoverability of the sample. Overall, the mechanical robustness and stability of FeCo@NiCo-LDH were sufficiently demonstrated in Figure S4.

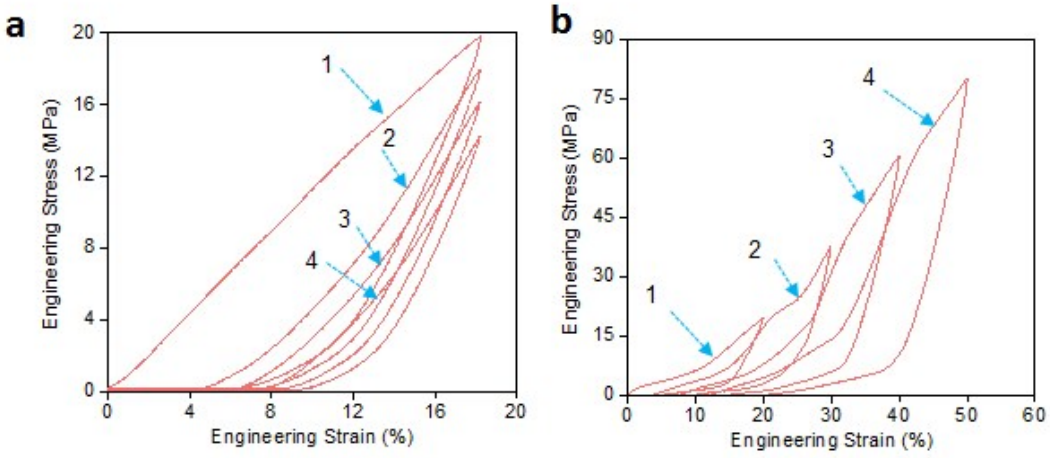

Figure S4. (a-b) Loading-unloading cyclic compression test of the FeCo@NiCo-LDH.

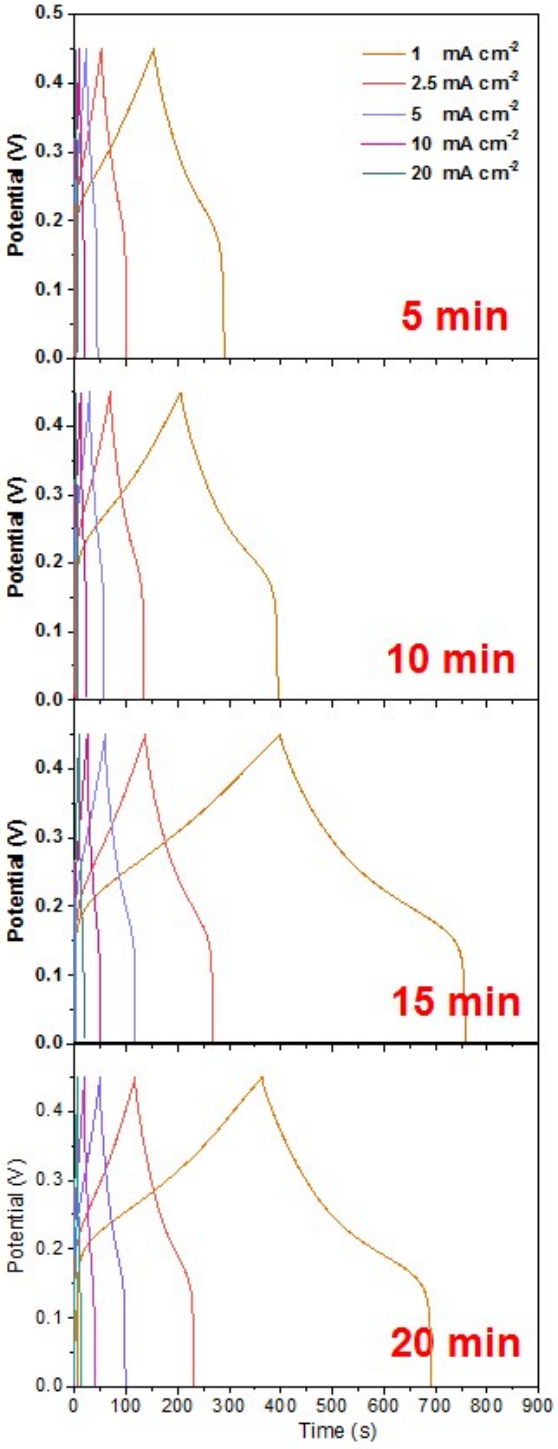

Figure S5. GCD curves of the FeCo-LDH electrodeposited on nickel foam for different times.

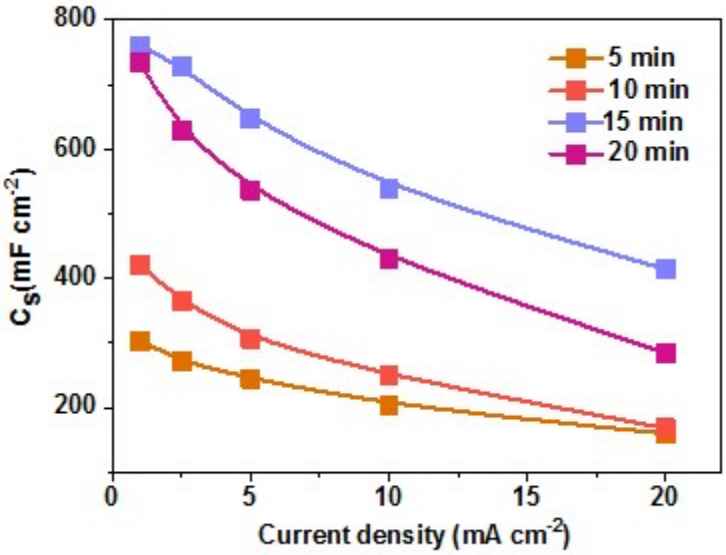

Figure S6. Areal capacitance (*Cs*) of the FeCo-LDH electrodeposited for different times at various current densities.

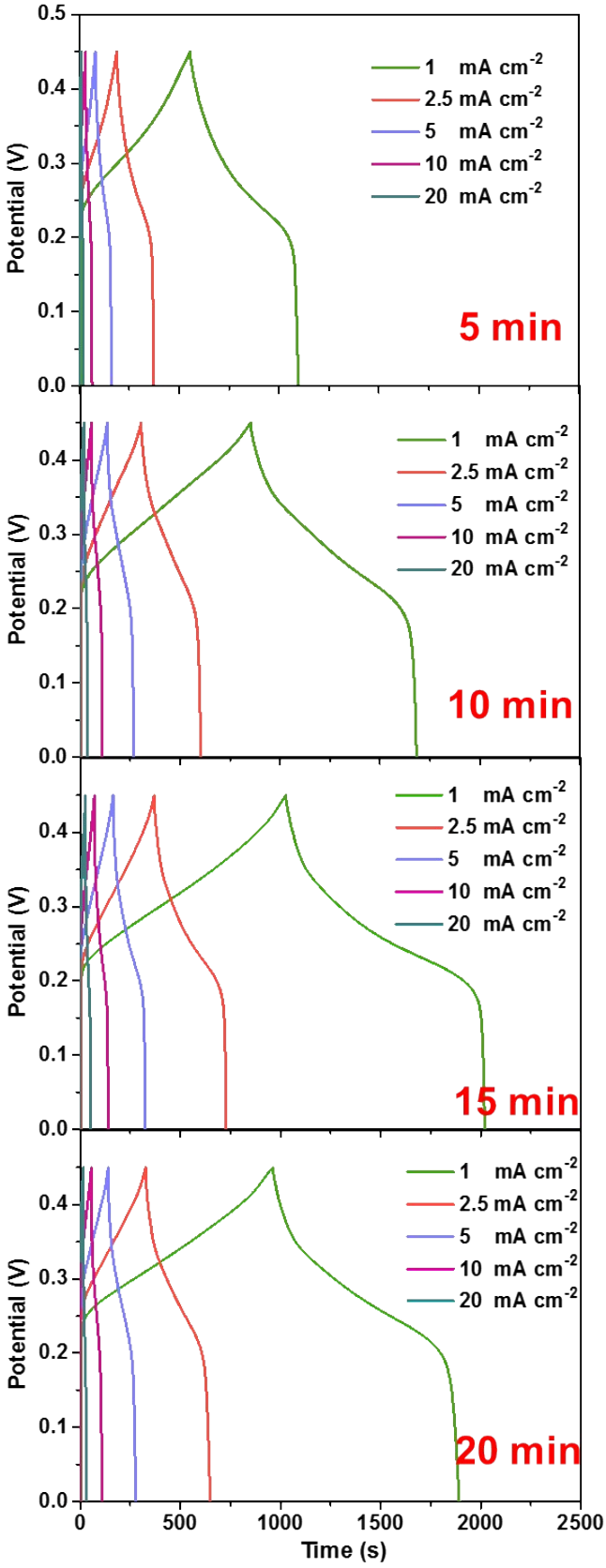

Figure S7. GCD curves of the FeCo@NiCo-LDH electrodeposited on nickel foam for different times.

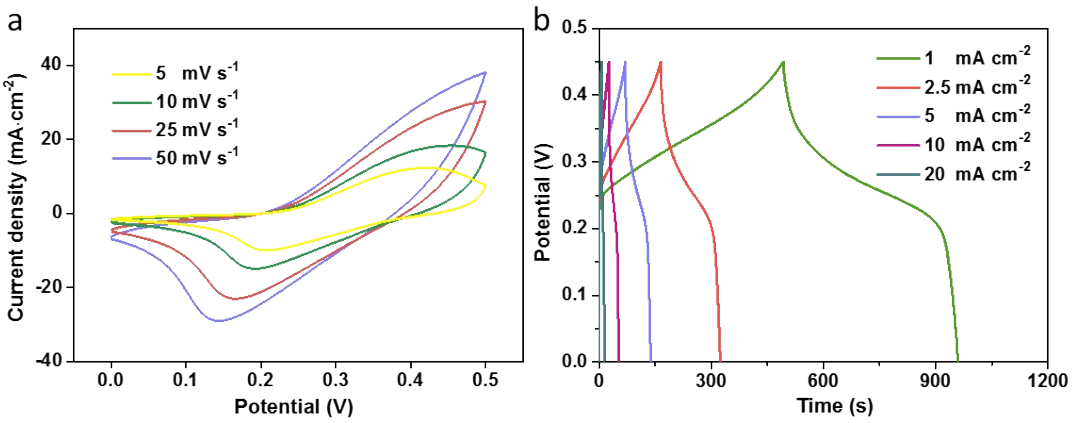

Figure S8. (a) CV curves and **(b)** GCD curves of NiCo-LDH deposited for 15 min**.**

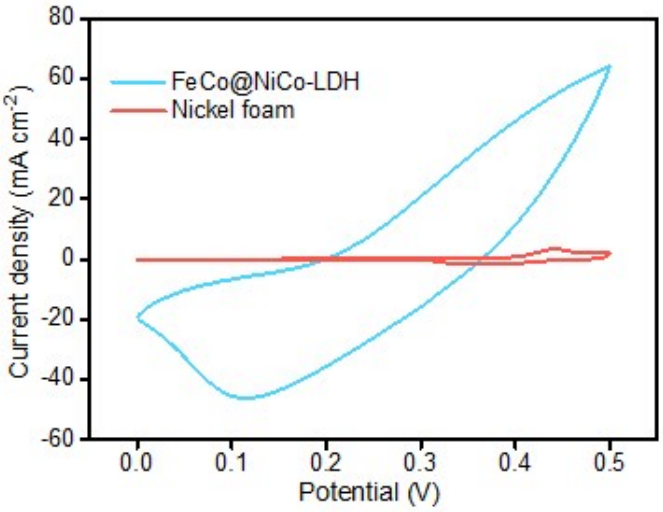

Figure S9. CV curves of FeCo@NiCo-LDH and pure nickel foam.

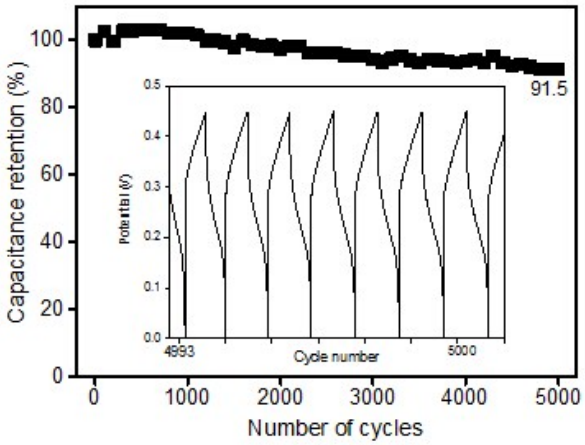

Figure S10. Cycle life of FeCo@NiCo-LDH at a current density of 20 mA cm^{-2} (Inset is the final GCD curves).

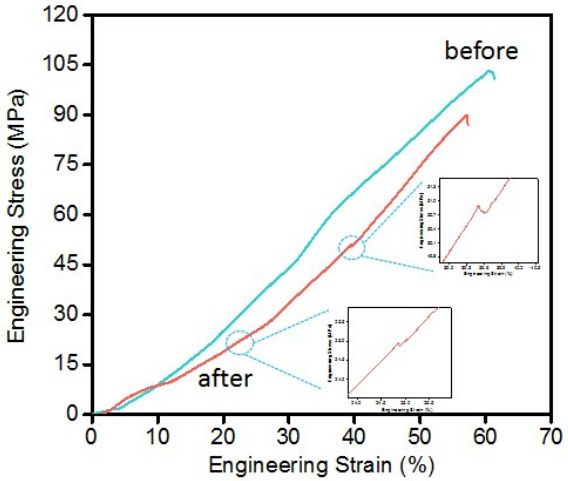

Figure S11. Comparison of the mechanical property of the FeCo@NiCo-LDH before and after cycling test.

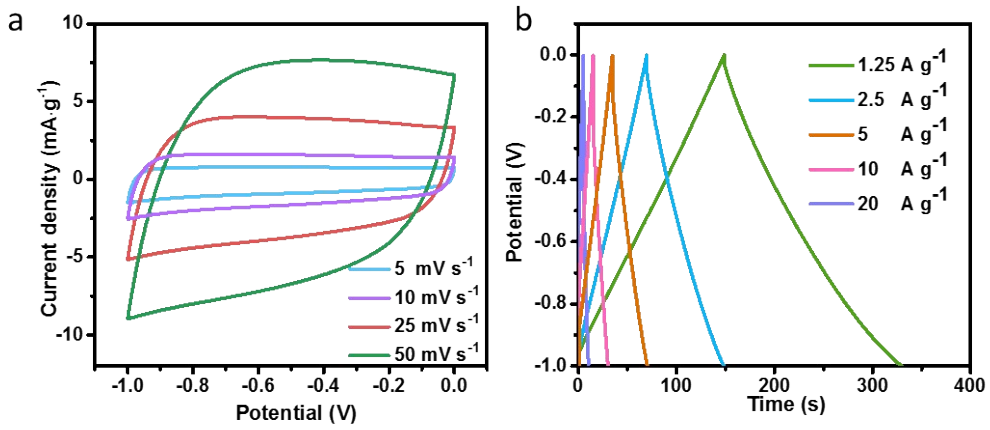

Figure S12. (a) CV curves and **(b)** GCD curves of AC.

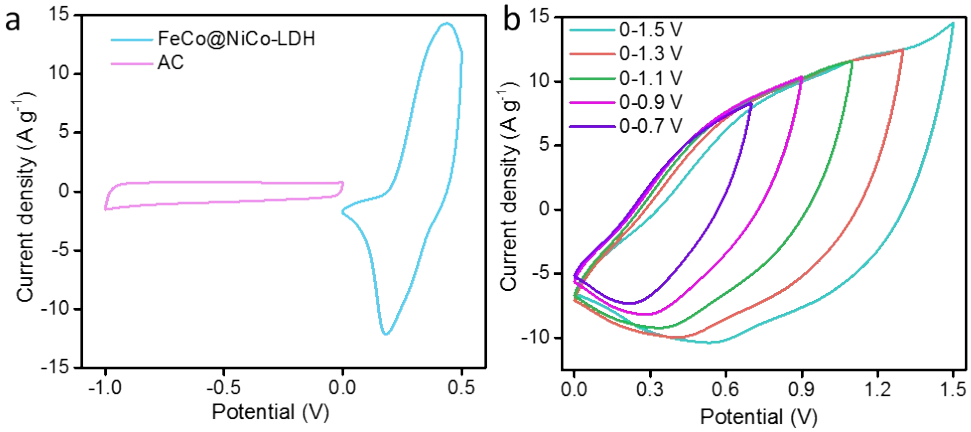

Figure S13. (a) CV curves of AC and FeCo@NiCo-LDH **(b)** CV curves of the assembled ASC at different potential range.

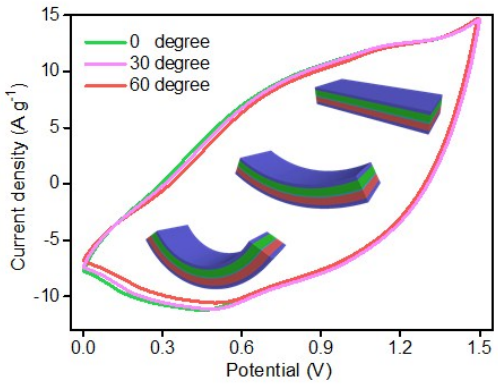

Figure S14. CV curves of the ASC under different bending degree.

Table S1. Comparative electrochemical characteristics of the FeCo@NiCo-LDH with previously reported LDH materials.

Electrode material	Fabrication method	Electrolyte	Current density	C (F/cm^2)	Ref.
NiCo LDH nanorods	Electrodeposition	1 M NaOH	1.26 mA cm^{-2}	0.13	[5]
MgAl LDH@RGO	In situ Solvothermal	1 M KOH	0.2 mA cm^{-2}	0.3	[6]
NiCo hydroxide	Electrodeposition	6 M KOH	1.25 mA cm^{-2}	0.4	[7]
NiCo LDH NSs	Electrodeposition	1 M KOH	1.28 mA cm^{-2}	0.6	[8]
NiAl LDH NSs	Hydrothermal	6 M KOH	1 mA cm^{-2}	0.84	[9]
NiCo binary hydroxide nanorods	Oil bath method	6 M KOH	3 mA cm^{-2}	1.03	[10]
NCo LDH/Ag nanowires	Electrodeposition	1 M KOH	1 mA cm^{-2}	1.1	[11]
NiCo LDH@$NiCo_2O_4$	Hydrothermal and Electrodeposition	1 M KOH	2 mA cm^{-2}	1.6	[12]
FeCo@NiCo LDH	Electrodeposition	2 M KOH	1 mA cm^{-2}	2.6	Our work

Supplementary Movie Captions

Movie S1. The device was used to power a digital watch.

Movie S2. The assembly was employed to drive 21 patterned red LED light.

Movie S3. The device can drive a small motor car for a long distance with charging only for 10 seconds.

Movie S4. 4 ASCs were able to successfully power 2 commercially available light bulbs.

Movie S5. After charging only for 10 seconds by harvesting the wind energy, the ASCs still can power the patterned LED light.

Reference

1 L. Mai, A. Minhas-Khan, X. Tian, K. M. Hercule, Y. Zhao, X. Lin and X. Xu, *Nat. Commun.*, 2013, **4**, 2923.

2 B. Zhao, D. Chen, X. Xiong, B. Song, R. Hu, Q. Zhang, B. H. Rainwater, G. H. Waller, D. Zhen, Y. Ding, Y. Chen, C. Qu, D. Dang, C.-P. Wong and M. Liu, *Energy Storage Mater.*, 2017, **7**, 32–39.

3 L. Gao, J. U. Surjadi, K. Cao, H. Zhang, P. Li, S. Xu, C. Jiang, J. Song, D. Sun and Y. Lu, *ACS Appl. Mater. Interfaces*, 2017, **9**, 5409–5418.

4 W. Hong, J. Wang, L. Niu, J. Sun, P. Gong and S. Yang, *J. Alloys Compd.*, 2014, **608**, 297–303.

5 F. Lai, Y. Huang, Y. E. Miao and T. Liu, *Electrochim. Acta*, 2015, **174**, 456–463.

6 G. Hatui, G. C. Nayak and G. Udayabhanu, *Electrochim. Acta*, 2016, **219**, 214–226.

7 M. Yang, H. Cheng, Y. Gu, Z. Sun, J. Hu, L. Cao, F. Lv, M. Li, W. Wang, Z. Wang, S. Wu, H. Liu and Z. Lu, *Nano Res.*, 2015, **8**, 2744–2754.

8 G. Nagaraju, G. S. R. Raju, Y. H. Ko and J. S. Yu, *Nanoscale*, 2016, **8**, 812–25.

9 M. Du, X. Yin, C. Tang, T. J. Huang and H. Gong, *Electrochim. Acta*, 2016, **190**, 521–530.

10 X. Sun, G. Wang, H. Sun, F. Lu, M. Yu and J. Lian, *J. Power Sources*, 2013, **238**, 150–156.

11 S. C. Sekhar, G. Nagaraju and J. S. Yu, *Nano Energy*, 2017, **36**, 58–67.

12 L. Huang, D. Chen, Y. Ding, S. Feng, Z. L. Wang and M. Liu, *Nano Lett.*, 2013, **13**, 3135–3139.